Progress in Natural Science: Materials International xxx (xxxx) xxx

HOSTED BY

ELSEVIER

Contents lists available at ScienceDirect

Progress in Natural Science: Materials International

journal homepage: www.elsevier.com/locate/pnsmi

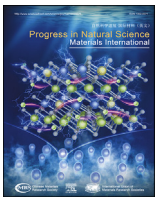

A universal and ultrafast method for fabricating a library of nanocellulose-supported metal nanoparticles

Ziyi Luo [a], Xiaoyang Wang [a], Baihua Cui [c], Hao Luo [a], Tao Zhang [a], Jia Ding [a], Yanan Chen [a,*], Yida Deng [b,**], Wenbin Hu [a]

[a] School of Materials Science and Engineering, Tianjin University, Tianjin, 300072, China
[b] State Key Laboratory of Marine Resource Utilization in South China Sea, School of Materials Science and Engineering, Hainan University, Haikou 570228, P.R. China
[c] Department of Chemistry, National University of Singapore, Singapore, 117543, Singapore

ARTICLE INFO

Keywords:
Nanoparticles
High-temperature shock
Nanocellulose
Nanomanufacturing
Hydrogen evolution reaction (HER)
Electrocatalysis

ABSTRACT

Using nanocatalysts to catalyze water electrolysis for hydrogen production is an ideal solution to address the energy crisis. The most well-adopted fabrication methods for nanocatalysts are tube furnace annealing, Hydrothermal method, etc., hardly satisfying the trade-off among coarsening, dispersity, and particle size due to mutual restrictions. Herein, a universal, ultrafast and facile cellulose nanometer whiskers-high temperature shock (CNW-HTS) method was reported for fabricating a library of ultrafine metal nanoparticles with uniform dispersion and narrow size distribution. The metal-anchor functional groups in CNW (i.e., –OH and –COOH) and the characteristics of the HTS method for ultrafast heating and powerful quenching synergistically contribute to the successful synthesis of metal nanoparticles. As an initial demonstration, the as-prepared Pt nanocatalyst (η10 mA cm^{-2} = 51.8 mV) shows more excellent catalytic hydrogen evolution reaction (HER) performance than the Pt catalyst prepared in the tubular furnace (η10 mA cm^{-2} = 169.4 mV). This rapid and universal CNW-HTS method can pave the way for nanomanufacturing to produce high-quality metal nanoparticles, thereby expanding applications of energy conversion and electrocatalysis.

1. Introduction

The world is confronting the problem of energy crises and environmental pollution. Thus, futuristic supplies are planned to gradually shift to renewables to find a sustainable, safer, and environment-friendly energy solution. Amongst these, hydrogen molecules (H_2) have carbon-free character and the highest energy density (≈146 MJ kg^{-1}), making H_2 to be widely recognized as one of the most promising alternatives in the next decade [3,4]. Water electrolysis powered by renewable energy sources to obtain hydrogen production is the ultimate ideal choice [14,17]. Wherein the hydrogen evolution reaction (HER) is a significant semi-reaction of water electrolysis. Efficient water splitting needs to develop highly active and durable electrocatalysts to diminish overpotentials for HER.

Pt has the highest turnover frequency (TOF) and its intrinsic activity exceeds any existing earth-abundant HER catalyst by at least three orders of magnitude [1], thus Pt and Pt-based electrocatalyst materials are considered the most suitable for industrial use. However, the scarcity of Pt reserves on Earth hinders its potential for scale-up commercialization. Therefore, the prime goal is to increase the Pt utilization efficiency while lowering the dosage of Pt. One strategy is synthesizing highly dispersed and homogeneously sized Pt nanoparticles (NPs) [18–22]. Owing to catalytic reactions being surface processes, decreasing the size of the catalyst to increase the surface area is an efficient approach to enhance the catalytic activity with minimized mass loading. The synthesis methods of Pt nanocatalysts can be divided into two categories: bottom-up [2,9] and top-down [16]. The synthesis of Pt nanoparticles by chemical reduction of Pt ions is called the "bottom-up" method, for instance, impregnation and atomic layer deposition. Wang et al. synthesized Pt NPs (2.8 nm) on a vanadium carbide nanosheet support (V_8C_7@C) via the ethylene glycol reduction method, with a Pt loading of 4.78 wt%. When applied to electrocatalytic HER, these Pt NPs exhibit excellent HER catalytic activity with an overpotential of 6 mV in 0.5 M H_2SO_4 and 55 mV in 1 M KOH at a current density of 10 mA cm^{-2} [10]. Mu et al. synthesized Pt@Ni ZIF-NC via dispersing Pt NPs (2.3 nm) on ZIF-NC, with an overpotential of 29 mV at a current density of 10 mA

* Corresponding author.
** Corresponding author.
E-mail addresses: jiading@tju.edu.cn (J. Ding), Yananchen@tju.edu.cn (Y. Chen), yd_deng@hainanu.edu.cn (Y. Deng), wbhu@tju.edu.cn (W. Hu).

https://doi.org/10.1016/j.pnsc.2024.04.006
Received 29 January 2024; Received in revised form 2 April 2024; Accepted 12 April 2024

cm^{-2} [11]. The synthesis method of using laser ablation or other methods to break large Pt bulk into nanoscale particles is called the "top-down" method. For example, Ruffino et al. synthesized Pt NPs, an average particle size of 10–15 nm, by Pulsed Laser Ablation (PLA) in a liquid environment [12]. Typically, the preparation of Pt nanocatalysts faces the issues of long synthesis cycles and aggregation of nanoparticles. The size effect of Pt has a significant impact on catalytic activity. The catalytic activity can get a huge boost with the size of the catalyst decreasing from 1 mm to 1 nm, due to the increase in S/V ratio [15]. The use of supporting materials for helping to disperse and stabilize Pt NPs is an effective strategy [23].

The nanocellulose is a natural polymer that can be extracted from wood, and most plant fibers, including cotton and hemp, which have the superiorities of wide sources, low price, environmental friendliness, and renewability [24,25]. Nanocellulose water suspension can form a three-dimensional network structure with a large specific surface area and multiple hydroxyl groups, providing loading sites for uniform dispersion of metal nanoparticles on the surface to construct composite catalyst materials [26–28]. In Shen et al.'s study, with metal ion (Co^{2+}) immobilized and chelated on the surface of cellulose nanocrystals CNC via hydroxyl groups, cobalt-adenine (CoA) coordination polymer with definite interaction of Co–N is self-assembled on the CNC skeletons (CoA@CNC) [13]. This catalyst demonstrates outstanding stability and bifunctional catalytic activity in the alkaline electrolyte for reversible oxygen reduction reaction (ORR) and oxygen evolution reaction (OER).

In this work, uniform Pt nanoparticles with an average diameter of around 4 nm were successfully formed on cellulose nanometer whiskers (CNW) carbonized by the high-temperature shock (HTS) method [5]. Fig. 1 compares the Pt/CNW carbonization processes of the HTS method and the traditional method. Generally, the heating process takes place in a horizontal tubular furnace (TF) for a long time, while the reaction proceeds in the direction of decreasing the Gibbs free energy of the system, resulting in Ostwald Ripening of Pt nanoparticles, poor particle dispersion and uneven particle size distribution of the products. The HTS method has the characteristics of an extremely fast heating rate (10^5 K s^{-1}) [6], short dwelling time (≈20 ms) [8], and powerful quenching (10^{14} K s^{-1}) [7], which avoids Oswald ripening of Pt NPs while rapidly carbonizing CNW. Accordingly, Pt/CNWC with a mass fraction of about 5.5 wt% synthesized by the HTS method has excellent HER catalytic performance. More significantly, the rapid CNW-HTS synthetic method is not only limited to the Pt NPs but also can be comfortably expanded to the synthesis of other metal nanoparticles. To verify the universality of this method, other uniformly sized and dispersed nanoparticles were successfully synthesized, such as Ag NPs, Cu NPs, Ru NPs, and Ir NPs. This study can make clear the new, fast, green, and general fabrication of metal nanocatalyst materials toward extending the path for their synthesis and application.

2. Experimental section

2.1. Materials

Deionized water was provided by the ultrapure water system (Milli-Q). Cellulose nanometer whiskers (CNW, 5 wt%) were purchased from North Century (Jiangsu) Cellulose Material Co. Ltd. H_2PtCl_6, $NaBH_4$, and polyvinyl pyrrolidone (PVP) were purchased from Sigma-Aldrich. All chemical reagents were used directly without further processing.

2.2. Synthesis of Pt/CNWC

For a typical synthesis of Pt/CNWC catalyst, 200 mg CNW and 4 mL of H_2PtCl_6 (20 mmol L^{-1}) solution were added to 20 mL PVP solution (20 mmol L^{-1}) and stirred at room temperature for 10 min to make a uniform dispersion. Then the pre-prepared $NaBH_4$ solution (10 mmol L^{-1}) was added to the above well-dispersed suspension and kept stirring for 5 min. Next, the Pt/CNW samples were collected by centrifugation at 10,000 rpm and subsequent washing with deionized water, followed by drying at 60 °C.

The as-prepared Pt/CNW was then carbonized by HTS under flowing Ar at 700 °C for less than 1 s. The as-synthesized samples were denoted as HT-Pt/CNWC. For comparison purposes, the samples were carbonized at the same temperature for 2 h in a horizontal tube furnace (at a heating rate of 5 °C min^{-1} under flowing Ar). The resulting samples were denoted as TF-Pt/CNWC.

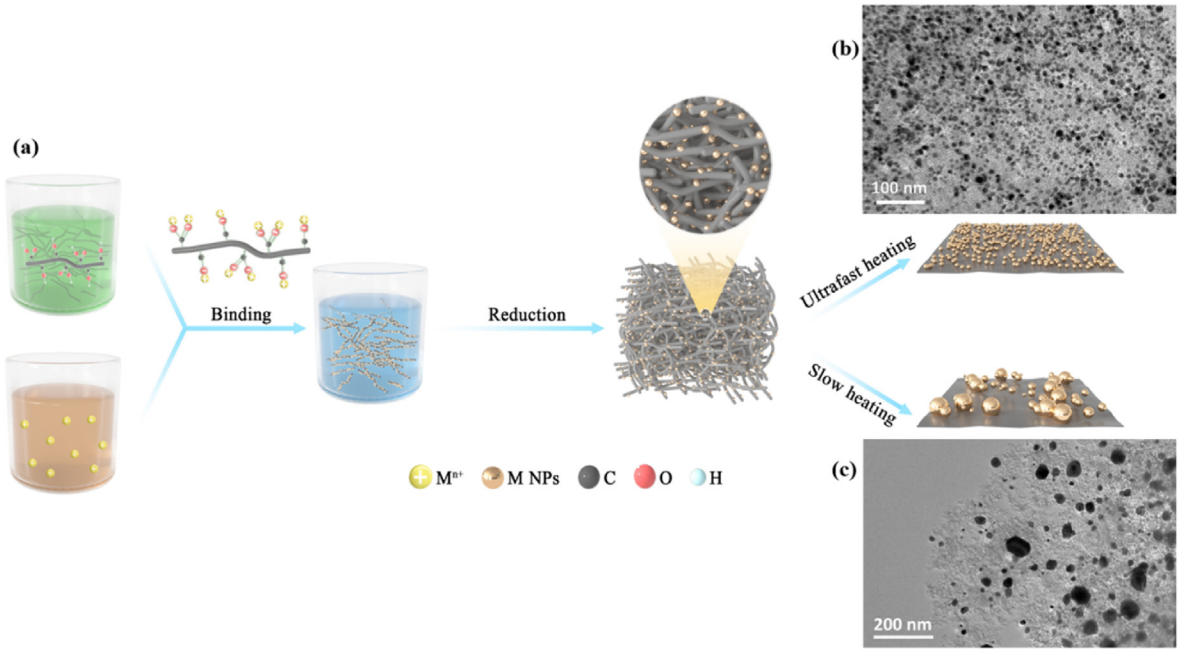

Fig. 1. (a) Schematic comparison between the HTS heating and traditional TF heating method for the CNW collaborative synthesis of metal nanoparticles. (b) TEM image of Pt NPs synthesized by HTS (HT-Pt/CNWC). (c) TEM image of Pt particles synthesized by TF (TF-Pt/CNWC).

2.3. Material characterization

Energy dispersive spectroscopy (EDS) and scanning electron microscopy (SEM) were performed using a JEOL JSM-7800F microscope. Raman spectroscopy is performed with Jobin-Yvon HR 800 to scatter and measure structural properties. High-Resolution Transmission Electron Microscope (HRTEM) was carried out on a JEOL JEM-ARM200F (accelerating voltage: 200 kV) transmission electron microscope. X-ray Diffraction (XRD) was conducted using the Bruker (Cu Kα radiation diffractometer, λ = 1.5406 Å) D8 Advanced X-ray diffractometer with a working voltage of 40 KV and working current of 40 mA. Using an Axis Supra X-ray photoelectron spectrometer (Kratos Analytical Ltd., UK) to perform X-ray photoelectron spectroscopy (XPS) measurements, with Al Kα ($h\nu = 1486.6$ eV) as the radiation source to achieve an energy resolution of $\Delta E \leq 0.5$ eV (C 1s = 284.8 eV). The loading amount of metallic Pt was obtained by thermogravimetry analysis using STA 449 F3(NETZSCH Ltd., GE).

2.4. Electrochemical measurement

The HER tests were conducted in a 0.5 M H_2SO_4 solution at room temperature. Using a glassy carbon electrode with an electrocatalysts-loaded area of 0.196 cm^2 as the working electrode, a graphite rod and a KCl-saturated Hg/Hg_2Cl_2 electrode were used as the counter and reference electrodes, respectively. The glassy carbon electrode needed to be polished with 1.0-, 0.3- and 0.05-μm alumina suspensions on a suede polishing cloth before measurements. The surface of the electrode should be checked at each step of polishing until the surface is as smooth as a mirror, then rinsed with deionized water several times. Weigh 2 mg of catalysts synthesized and 2 mg of carbon black, suspended in 10 μl of Nafion solution (5 wt%, Du Pont) and 500 μl of isopropanol afterward, then followed by ultrasonication for 1 h to obtain a homogeneous ink. Load the 15 μl of catalyst ink on a glassy carbon electrode surface homogeneously and dry at room temperature for testing. All the electrochemical measurements were performed by the electrochemical workstation CHI660E. Firstly, the samples should be electrochemically activated before electrochemical measurements, which perform the cyclic voltammetry (CV) to scan potential until it reaches stability. The scanning potential range is 0.0 V to −0.8 V (vs. SCE) with scanning rates of 100, 50, and 20 mV s^{-1}, and cycle 10 times at each scanning rate. Subsequently, the linear sweep voltammetry (LSV) curve of the sample is recorded at a scan rate of 5 mV s^{-1} within the same potential range. The electrochemical impedance spectroscopic (EIS) analysis was carried out with a frequency range of 1 M Hz to 0.1 Hz at η10 mA cm^{-2} with an oscillation potential amplitude of 50 mV from the equilibrium for all two fabricated working electrodes. The HER stability of the catalyst was evaluated using the continuous chronoamperometry measurement and tested the i-t curve of the sample at a potential of −0.055 V (vs. RHE, at 10 mA cm^{-2}).

3. Result and discussion

Fig. 1a shows the two-step synthesis process of the Pt/CNWC catalyst. In the first step, CNW with rich –OH and –OOH groups is used as a carrier to immobilize Pt^{4+}, and then the $NaBH_4$ is added to reduce Pt^{4+}. The product is separated from the suspension and dried at 60 °C in an oven. The oven drying is an inefficient drying process. Due to the strong intermolecular hydrogen bonds between CNW molecules and the attraction and reorganization of the hydroxyls on the surface, it will form a continuous fiber network during drying (i.e., hornification) [29–31]. Therefore, it is transformed into thin nanosheets after HTS heating for carbonization. Subsequently, the product is subjected to carbonization at 700 °C (under Ar atmosphere) by HTS to obtain HT-Pt/CNWC. For comparison, slow heating was carried out in a tube furnace for 1 h under the same conditions (Ar atmosphere, 700 °C), resulting in TF-Pt/CNWC. The SEM image of unloaded and uncarbonized cellulose nano whiskers (CNW) with conductive coatings is shown in Fig. 2a, indicating that CNW has a nanorod-like structure. Fig. 2b shows the Pt NPs with even particle size were prepared facilely by ultrafast HTS process. The average particle size of Pt NPs is 4.04 ± 0.83 nm according to the statistical analysis of size distribution in Fig. S1. In addition, Fig. 2b also shows that the CNW nanorods transform into thin nanosheets after HTS heating because of the hornification in CNW. A high-resolution transmission electron microscopy (HRTEM) image displays Pt NPs have almost no defects and the exposure facets of Pt NPs are identified as (200) (Fig. 2c). The Pt nanoparticles are uniformly dispersed in the CNWC, as evidenced by energy-dispersive spectroscopy (EDS) elemental mapping (on the right side of Fig. 2c). The TEM image of TF-Pt/CNWC samples (Fig. 2d) in the tube furnace clearly demonstrates the obvious agglomeration and coarsening of Pt NPs.

The specific Pt loading on CNWC substrate was determined by Thermogravimetry Analysis (TGA), the mass fraction in HT-Pt/CNWC is 5.5 % (Fig. 3a). The typical XRD patterns of the Pt/CNW and HT-Pt/CNWC are shown in Fig. 3b. The diffraction peaks at 14.9° (d = 5.9 Å), 16.5° (d = 5.4 Å), 22.8° (d = 3.9 Å) and 34.2° (d = 2.6 Å) were corresponded to the (10), (110), (200), and (004) crystal facets of CNW crystallization, respectively. Fig. 3b confirms that the CNW was not completely carbonized to amorphous carbon after HTS and retains a small amount of crystallinity. A range of peaks observed at 39.8° (d = 2.3 Å), 46.4° (d = 2.0 Å) and 67.7° (d = 1.4 Å) respectively correspond to the (110), (200), and (004) crystal facets of face-centered cubic (*fcc*) structure Pt (PDF# 87–0640). This finding is in accord with the reduction of the H_2PtCl_6 to metallic Pt. Meanwhile, the peak observed at 31.6° (d = 2.8 Å) may result from either oxidized CNWs or PtO_x species. The Scherrer relation was used to calculate the average diameter of the HT-Pt/CNWC nanoparticles:

$$D = k\lambda/(\beta\cos\theta),$$

where λ = 1.54056 Å is the CuKα radiation, θ is the Bragg angle, β is the half-maximum width (FWHM) of the diffraction peak, K is the shape factor which is approximately 0.89, and D is the average diameter that needs to be calculated. After calculation, D = 5.3 nm in line with the result of TEM is obtained, which further confirms the even size distribution and small size of Pt NPs in the HT-Pt/CNWC.

Fig. 3c presents the Raman spectra of Pt/CNW and HT-Pt/CNWC. Prominent Raman bands at ~1100, ~1800, ~2062 and ~2884 cm^{-1} were observed in Pt/CNW. The most important peaks in the spectrum occurred at ~1100–1800, and ~2062 cm^{-1}. These peaks are respectively attributed to C–O–C, O–H and C═O vibrations, derived from the hydroxyl and carboxyl groups in CNW. The other peak was observed at ~2884 cm^{-1} arising from C–H. The peaks related to hydroxyl and carboxyl groups significantly weakened after HTS. The peaks of D and G bands are observed respectively at ~1350 and ~1585 cm^{-1} for HT-Pt/CNWC in Fig. 3c. The D-band reflects the defects and disorder of carbon materials. Therefore, the broad D-band indicates that the CNWC has a low degree of order. And the I_D/I_G (the ratio of D-band to G-band intensity) is 2.3, suggesting that CNW becomes amorphous carbon after the HTS process.

To further investigate the chemical state and chemical bond properties of carbon and Pt on the surface, we performed a spectral analysis of the materials by XPS. Figs. S2–S4 show the survey spectra of Pt/CNW, HT-Pt/CNWC and TF/CNWC. We presume that the presence of contaminants (Si, Na) may be associated with the measurements, i.e., it represents the residual contamination of the substrate. The high-resolution XPS C1s and O 1s spectra of Pt/CNW samples are shown in Fig. S5. The main peaks are polyaromatic carbon (C–C/C═C), aliphatic carbon and hydroxyl carbon (C–H&C–O), two carbon atoms connected to a single oxygen atom (C–O–C) and carboxylic carbon (O–C═O), which is in line with the results of Raman spectroscopy. Both C1s and Raman spectra have demonstrated the presence of a large number of –OH and –COOH functional groups in CNW. Therefore, metal particles can be stabilized on

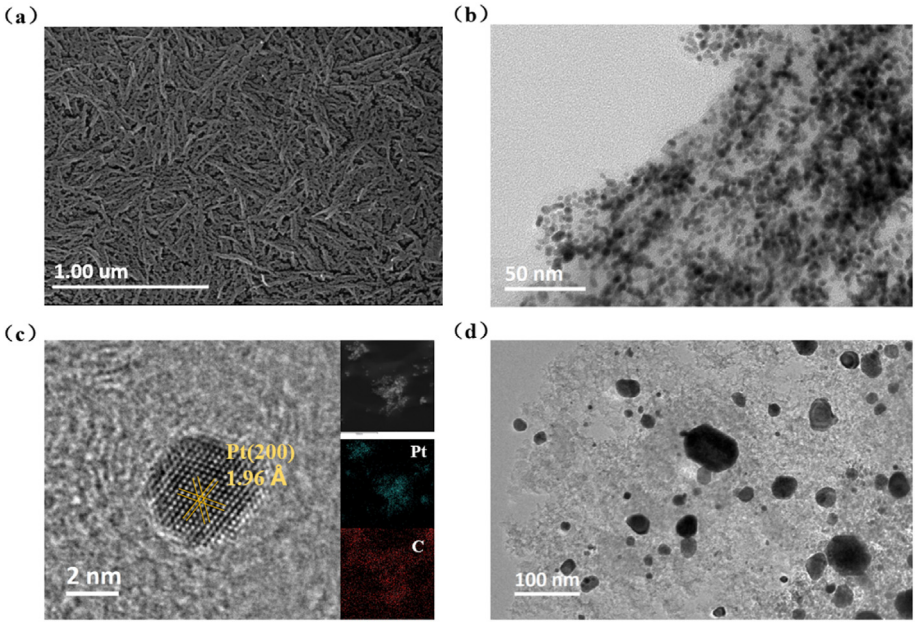

Fig. 2. (a) SEM image of raw CNW. (b) and (c) TEM and EDS-elemental mapping images of HT-Pt/CNWC. (d) TEM image of TF-Pt/CNWC.

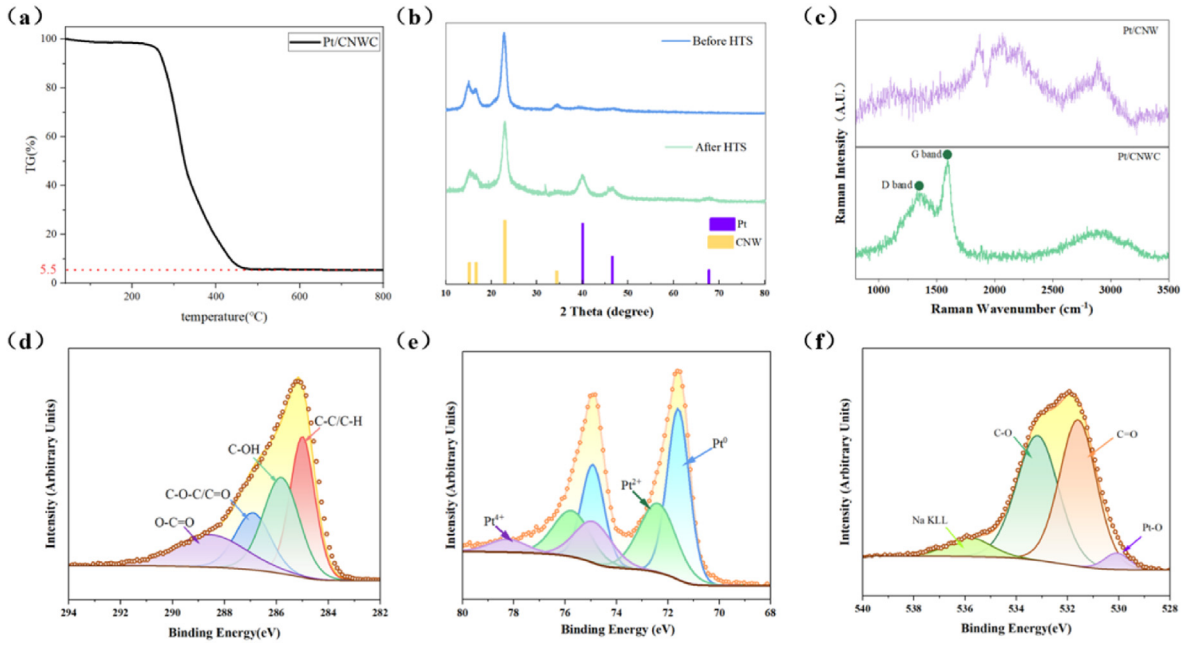

Fig. 3. (a) TGA curve of HT-Pt/CNWC. (b) XRD patterns of Pt/CNW and HT-Pt/CNWC. (c) Raman curves of Pt/CNW and HT-Pt/CNWC. High energy resolved XPS spectra: (d) – C 1s, (e) – Pt 4f, and (f) – O 1s of HT-Pt/CNWC.

cellulose surfaces through oxygen-metal electrostatic interactions. High-resolution XPS C 1s spectra of HT-Pt/CNWC and TF-Pt/CNWC are respectively presented in Fig. 3d and Fig. S6. After heating, the peak intensities of C–O and C═O were significantly reduced, and C–C became the highest peak, indicating the completion of carbonization. Comparing the C1s spectra of HTS-treated and TF-treated CNW, it is established that the TF- treated sample has a higher degree of carbonization. Fig. 3e shows the High-resolution XPS Pt 4f spectra of the product formed by HTS, which features the usual spin–orbit splitting. Two pairs of high-intensity doublet peaks observed at 71.6 eV (Pt $4f_{7/2}$) and 74.9 eV (Pt $4f_{5/2}$) are ascribed to metallic Pt. Two pairs of peaks observed at 72.4 eV (Pt $4f_{7/2}$) and 75.7 eV (Pt $4f_{5/2}$) are ascribed to Pt (II). Additionally, a pair of low-intensity doublet peaks were observed at 74.9 eV (Pt $4f_{7/2}$) and 78.2 eV (Pt $4f_{5/2}$), and this was due to Pt (IV). These results are consistent with the XRD results, indicating that H_2PtCl_6 has been successfully reduced to metallic Pt, with a small amount of Pt (II) and Pt (IV) species present due to surface oxidation. As seen in Fig. 3f, the peak at 530 eV belongs to the Pt–O bond.

The HER performance of the prepared catalysts was tested in a standard three-electrode system without insulation resistance compensation, and the loading mass was 0.3 mg cm^{-2}. As shown in Fig. 4a, HT-Pt/CNWC exhibited the superior HER performance with a low overpotential, only 51.8 mV at a current density of 10 mA cm^{-2}, which is much better than that of TF-Pt/CNWC (169.4 mV). In addition, the Tafel slope gives a lower value of HT-Pt/CNWC (50 mV dec^{-1}) than that of TF-Pt/CNWC (270 mV dec^{-1}), indicating faster reaction kinetics for HT-Pt/

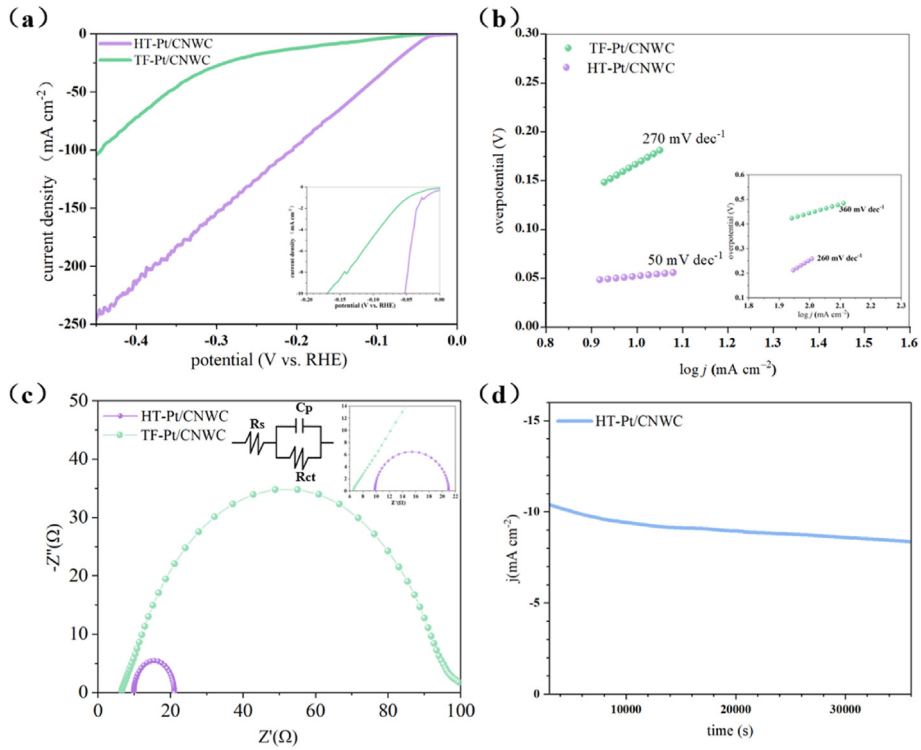

Fig. 4. The electrochemical performance of the electrocatalysts prepared in this study, and all electrochemical tests are conducted in 0.5 M H_2SO_4. (a) The LSV curves. (b) Corresponding Tafel slopes. (c) EIS Nyquist plots of HT-Pt/CNWC and comparative samples; the inset shows the equivalent circuit diagram. (d) chronoamperometry measurement of HT-Pt/CNWC at a potential of −0.055 V (vs RHE, at 10 mA cm^{-2}) in 0.5 M H_2SO_4.

CNWC (Fig. 4b). Under high current density (100 mA cm^{-2}, Fig. 4b inset), the HT-sample still maintains a relatively low Tafel slope of 260 mV dec^{-1} in comparison with the TF-sample (360 mV dec^{-1}). EIS analyses were conducted on both the HT-Pt/CNWC and the TF-Pt/CNWC to investigate the changes in electrocatalytic properties at η10 mA cm^{-2}. Fig. 4c shows various Nyquist plots with the corresponding electronic equivalent circuit fit (EEC Fit). Two resistances are considered in the EEC Fit. Rs, Rct and Cp respectively represent series resistance, charge transfer resistance and double-layer capacitance. As for the hydrogen evolution process, Rct can be directly related to the rate of the charge transfer process at the interface of electrocatalysts. The smaller the Rct of the test object, the faster the charge transfer rate, resulting in a lower required overpotential. HT-Pt/CNCW showed a smaller diameter semicircle, indicating the minimal Rct (6 Ω), which was only 14.3 % of TF-Pt/CNWC's (the enlarged inset of Fig. 4c). The curve in Fig. 4d is the stability test of the HT sample. After 30,000 s of continuous chronoamperometry measurement at a potential of −0.055 V (vs RHE, at 10 mA cm^{-2}), the current density of HT-Pt/CNWC decreases by ~15 %.

4. The universality of HTS technique for synthesizing metal NPs/CNWC

More crucially, in addition to being used for synthesizing Pt NPs, the CNW-HTS synthetic method also can easily be applied to the synthesis of other metal nanoparticles. This method has created more opportunities for the rapid synthesis and widespread application of metal nanoparticles with catalytic activity. To verify the universality of this CNW-HTS technique, other high-quality metal nanoparticles were successfully synthesized, such as Ag, Cu, Ir and Ru. XRD patterns of the HTS-fabricated Cu and Ag metal nanoparticles can match well with the corresponding standard cards, confirming that the precursors were successfully transformed into metal nanoparticles after the HTS treatment (Fig. S7). The XRD patterns of Ir and Ru NPs hardly observe corresponding metal peaks by reason of the extremely small particle size.

Fig. 5 shows the TEM and HRTEM images of the Ag/CNWC, Cu/CNWC, Ir/CNWC, and Ru/CNWC at different magnifications. Numerous nanoparticles are evenly distributed on carbonized CNW with average particle sizes of 7.77 nm for Ag, 32.53 nm for Cu, 1.44 nm for Ir and 2.74 nm for Ru (Fig. S8). Specifically, a large number of Cu cubes were observed in the TEM image of the HT-Cu/CNWC sample. It is speculated that the formation of Cu cubes may be due to the ligand effect of CNW, which selectively adsorbs on the surface of Cu nanoparticles. More in-depth research is needed to reveal the synthetic mechanism. Based on the high generality and efficiency of this HTS synthetic technique, and the binding effect of CNW, we were able to produce highly dispersed and uniformly sized metal nanomaterials in an ultra-short period. This ability to rapidly prepare an extensive range of ultrafine and uniform metal nanoparticles reveals the universality of our highly effective strategy for manufacturing metal nanocatalysts.

5. Conclusion

In summary, a general, green and ultrafast CNW-HTS method is developed for the fabrication of high-quality metal nanoparticles. The distinctive properties (i.e., Ultrahigh heating rates, powerful quenching and short dwelling time) of the HTS heating guarantee the successful production of ultrafine metal nanoparticles with uniform dispersion and narrow particle size distribution, which is beneficial to exceed the intrinsic imperfections of the traditional TF heating method. As a validation, we utilize the HTS strategy to rapidly synthesize Pt/CNWC. The obtained HT-Pt/CNWC delivers a superior electrocatalytic performance (51.8 mV at 10 mA cm^{-2}) than that of TF-Pt/CNWC (169.4 mV at 10 mA cm^{-2}) in HER. Additionally, the CNW-HTS synthetic approach demonstrates its universality and versatility by flexibly preparing other metal nanoparticles, such as Ag, Cu, Ir and Ru. This work can open up a new path for the ultrafast nanomanufacturing of metal nanocatalysts, which can effectively overcome the shortcomings of traditional methods.

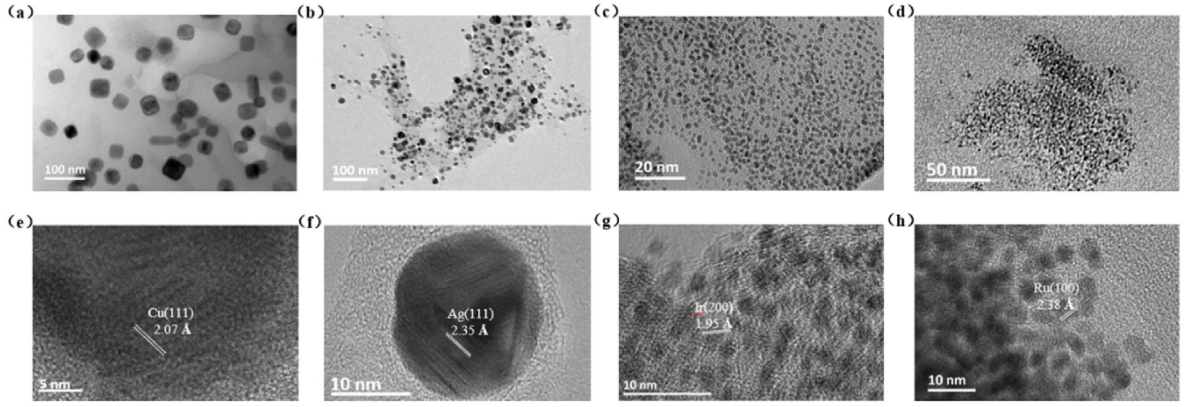

Fig. 5. The TEM pictures of (a), (e) Cu/CNWC. (b), (f) Ag/CNWC. (c), (g) Ir/CNWC. (d), (h) Ru/CNWC.

CRediT authorship contribution statement

Ziyi Luo: Conceptualization, Writing – original draft, Writing – review & editing. **Xiaoyang Wang:** Data curation, Writing – review & editing. **Baihua Cui:** Writing – review & editing. **Hao Luo:** Data curation. **Tao Zhang:** Conceptualization, Data curation. **Jia Ding:** Methodology. **Yanan Chen:** Conceptualization, Methodology, Supervision. **Yida Deng:** Methodology, Supervision. **Wenbin Hu:** Resources.

Declaration of competing interest

The authors declare that they have no known competing financial interests or personal relationships that could have appeared to influence the work reported in this paper.

Appendix A. Supplementary data

Supplementary data to this article can be found online at https://doi.org/10.1016/j.pnsc.2024.04.006.

References

[1] J.N. Hansen, H. Prats, K.K. Toudahl, N.M. Secher, K. Chan, J. Kibsgaard, I. Chorkendorff, Is there anything better than Pt for HER, ACS Energy Lett. 6 (2021) 1175–1180, https://doi.org/10.1021/acsenergylett.1c00246.

[2] S. Xu, Y. Kim, J. Park, D. Higgins, S.J. Shen, P. Schindler, D. Thian, J. Provine, J. Torgersen, T. Graf, T.D. Schladt, M. Orazov, B.H. Liu, T.F. Jaramillo, F.B. Prinz, Extending the limits of Pt/C catalysts with passivation-gas-incorporated atomic layer deposition, Nat. Catal. 1 (2018) 624–630, https://doi.org/10.1038/s41929-018-0118-1.

[3] W. Luo, Y. Wang, C. Cheng, Ru-based electrocatalysts for hydrogen evolution reaction: recent research advances and perspectives, Mater. Today Phy. 15 (2020) 100274, https://doi.org/10.1016/j.mtphys.2020.100274.

[4] F. Guo, T.J. Macdonald, A.J. Sobrido, L. Liu, J. Feng, G. He, Recent advances in ultralow-Pt-loading electrocatalysts for the efficient hydrogen evolution, Adv. Sci. 10 (2023) 2301098, https://doi.org/10.1002/advs.202301098.

[5] R. Jiang, Y. Da, X. Han, Y. Chen, Y. Deng, W. Hu, Ultrafast synthesis for functional nanomaterials, Cell Rep. Phys. Sci. 2 (2021) 100302, https://doi.org/10.1016/j.xcrp.2020.100302.

[6] Y. Yao, Z. Huang, P. Xie, S.D. Lacey, R.J. Jacob, H. Xie, F. Chen, A. Nie, T. Pu, M. Rehwoldt, D. Yu, M.R. Zachariah, C. Wang, R.S. Yassar, J. Li, L. Hu, Carbothermal shock synthesis of high-entropy-alloy nanoparticles, Science 359 (2018) 1489–1494. https://www.science.org/doi/10.1126/science.aan5412.

[7] L. Zhong, J. Wang, H. Sheng, Z. Zhang, S.X. Mao, Formation of monatomic metallic glasses through ultrafast liquid quenching, Nature 512 (2014) 177–180, https://doi.org/10.1038/nature13617.

[8] S. Liu, Y. Shen, Y. Zhang, B. Cui, S. Xi, J. Zhang, L. Xu, S. Zhu, Y. Chen, Y. Deng, W. Hu, Extreme environmental thermal shock induced dislocation-rich Pt nanoparticles boosting hydrogen evolution reaction, Adv. Mater. 34 (2022) 2106973, https://doi.org/10.1002/adma.202106973.

[9] Q. Yang, H. Liu, P. Yuan, Y. Jia, L. Zhuang, H. Zhang, X. Yan, G. Liu, Y. Zhao, J. Liu, S. Wei, L. Song, Q. Wu, B. Ge, L. Zhang, K. Wang, X. Wang, C.R. Chang, X. Yao, Single carbon vacancy traps atomic platinum for hydrogen evolution catalysis, J. Am. Chem. Soc. 144 (2022) 2171–2178, https://doi.org/10.1021/jacs.1c10814.

[10] W. Ma, J. Wan, W. Fu, Y. Wu, Y. Wang, H. Zhang, Y. Wang, Heterostructures induced between platinum nanoparticles and vanadium carbide boosting hydrogen evolution reaction, Appl. Catal. Gen. 633 (2022) 118512, https://doi.org/10.1016/j.apcata.2022.118512.

[11] L. Liang, H. Jin, H. Zhou, B. Liu, C. Hu, D. Chen, J. Zhu, Z. Wang, H.W. Li, S. Liu, D. He, S. Mu, Ultra-small platinum nanoparticles segregated by nickle sites for efficient ORR and HER processes, J. Energy Chem. 65 (2022) 48–54, https://doi.org/10.1016/j.jechem.2021.05.033.

[12] M. Censabella, V. Torrisi, S. Boninelli, C. Bongiorno, M.G. Grimaldi, F. Ruffino, Laser ablation synthesis of mono- and bimetallic Pt and Pd nanoparticles and fabrication of Pt-Pd/Graphene nanocomposites, Appl. Surf. Sci. 475 (2019) 494–503, https://doi.org/10.1016/j.apsusc.2019.01.029.

[13] M. Shen, K. Gao, F. Xiang, B. Wang, L. Dai, L. Zheng, F. Baker, C. Duan, Y. Zhang, S. Sun, Y. Ni, Nanocellulose-assisted synthesis of ultrafine Co nanoparticles-loaded bimodal micro-mesoporous N-rich carbon as bifunctional oxygen electrode for Zn-air batteries, J. Power Sources 450 (2020) 227640, https://doi.org/10.1016/j.jpowsour.2019.227640.

[14] J. Chi, H. Yu, Water electrolysis based on renewable energy for hydrogen production, Chin. J. Catal. 39 (2018) 390–394, https://doi.org/10.1016/S1872-2067(17)62949-8.

[15] S. Khamgaonkar, M. Okasha, V. Maheshwari, Recent advances towards increasing the Pt utilization efficiency for hydrogen evolution reaction: a review, Inorg. Chem. Front. 10 (2023) 6812–6848, https://doi.org/10.1039/D3QI01656K.

[16] J. Fichtner, S. Watzele, B. Garlyyev, R.M. Kluge, F. Haimerl, H.A. El-Sayed, W.J. Li, F.M. Maillard, L. Dubau, R. Chattot, J. Michalička, J.M. Macak, W. Wang, D. Wang, T. Gigl, C. Hugenschmidt, A.S. Bandarenka, Tailoring the oxygen reduction activity of Pt nanoparticles through surface defects: a simple top-down approach, ACS Catal. 10 (2020) 3131–3142, https://doi.org/10.1021/acscatal.9b04974.

[17] J. Zhou, X. Meng, Y. Chen, Research on DC power supply for electrolytic water to hydrogen based on renewable energy, J. Phys. Conf. 2465 (2023) 012007. https://iopscience.iop.org/article/10.1088/1742-6596/2465/1/012007.

[18] G. Ma, X. Zhang, G. Zhou, X. Wang, Hydrogen production from methanol reforming electrolysis at NiO nanosheets supported Pt nanoparticles, Chem. Eng. J. 411 (2021) 128292, https://doi.org/10.1016/j.cej.2020.128292.

[19] J. Han, C. Gong, C. He, P. He, J. Zhang, Z. Zhang, Sub-1 nm Pt nanoclusters on N and P co-doped carbon nanotubes for the electrocatalytic hydrogen evolution reaction, J. Mater. Chem. A 10 (2022) 16403–16408, https://doi.org/10.1039/d2ta05241e.

[20] X. Mo, K.C. Chan, E.C.M. Tse, A scalable laser-assisted method to produce active and robust graphene-supported nanoparticle electrocatalysts, Chem. Mater. 31 (2019) 8230–8238, https://doi.org/10.1021/acs.chemmater.9b03669.

[21] H. Xiao, Ji Zhang, M. Zhao, J. Ma, Y. Li, T. Hu, Z. Zheng, J. Jia, H. Wu, Electric field-assisted synthesis of Pt, carbon quantum dots-coloaded graphene hybrid for hydrogen evolution reaction, J. Power Sources 451 (2020) 227770, https://doi.org/10.1016/j.jpowsour.2020.227770.

[22] Z. Zeng, S. Küspert, S.E. Balaghi, H.E.M. Hussein, N. Ortlieb, M.K. Buß, P. Hügenell, S. Pollitt, N. Hug, J. Melke, A. Fischer, Ultrahigh mass activity Pt entities consisting of Pt single atoms, clusters, and nanoparticles for improved hydrogen evolution reaction, Small 19 (2023) 2205885, https://doi.org/10.1002/smll.202205885.

[23] W. Zhou, J. Jia, J. Lu, L. Yang, D. Hou, G. Li, S. Chen, Recent developments of carbon-based electrocatalysts for hydrogen evolution reaction, Nano Energy Nano Environ. 28 (2016) 29–43, https://doi.org/10.1016/j.nanoen.2016.08.027.

[24] Q. Zhang, L. Zhang, W. Wu, H. Xiao, Methods and applications of nanocellulose loaded with inorganic nanomaterials: a review, Carbohydrate Polymers 229 (2020) 115454, https://doi.org/10.1016/j.carbpol.2019.115454.

[25] K. Du, D. Zhang, S. Zhang, K.C. Tam, Advanced functionalized materials based on layer-by-layer assembled natural cellulose nanofiber for electrodes: a review, Small (2023) 2304739, https://doi.org/10.1002/smll.202304739.

[26] Y. Lu, G. Ye, X. She, S. Wang, D. Yang, Y. Yin, Sustainable route for molecularly thin cellulose nanoribbons and derived nitrogen-doped carbon electrocatalysts, ACS Sustainable Chem. Eng. 5 (2017) 8729–8737. https://hfbic1b13095ec5284139swokx5punnkck6fqffiac.eds.tju.edu.cn/10.1021/acssuschemeng.7b01511.

[27] W. Zhang, J. Chu, S. Li, Y. Li, L. Li, CoNxC active sites-rich three-dimensional porous carbon nanofibers network derived from bacterial cellulose and bimetal-ZIFs as efficient multifunctional electrocatalyst for rechargeable Zn–air batteries,

J. Energy Chem. 51 (2020) 323–332, https://doi.org/10.1016/j.jechem.2020.04.067.

[28] M. Chen, S. Deng, Y. Qing, H. Xu, Y. Liao, L. Li, Z. Zhang, N. Yan, C. Tian, Y. Wu, Y. Wu, Approaching well-dispersed MoS2 assisted with cellulose nanofiber for highly durable hydrogen evolution reaction, Carbohydrate Polymers 294 (2022) 119754, https://doi.org/10.1016/j.carbpol.2022.119754.

[29] C. Borsoi, M.V.G. Zimmernnam, A.J. Zattera, R.M.C. Santana, C.A. Ferreira, Thermal degradation behavior of cellulose nanofibers and nanowhiskers, J. Therm. Anal. Calorim. 126 (2016) 1867–1878. https://link.springer.com/article/10.1007/s10973-016-5653-x.

[30] J.M.B. Fernandes Diniz, M.H. Gil, J.A.A.M. Castro, Hornification—its origin and interpretation in wood pulps, Wood Sci. Technol. 37 (2004) 489–494. https://link.springer.com/article/10.1007/s00226-003-0216-2.

[31] Y. Peng, D.J. Gardner, Y. Han, Drying cellulose nanofibrils: in search of a suitable method, Cellulose 19 (2012) 91–102. https://link.springer.com/article/10.1007/s10570-011-9630-z.